

1-28-2020

## Aromatic Ouroboroi: Heterocycles Involving a Sigma-Donor-Acceptor Bond and $4n+2$ Pi-Electrons

Kelling J. Donald  
*University of Richmond*

William Tiznado  
*Universidad Andres Bello, Chile*

Rodrigo Baez-Grez

Diego Inostroza

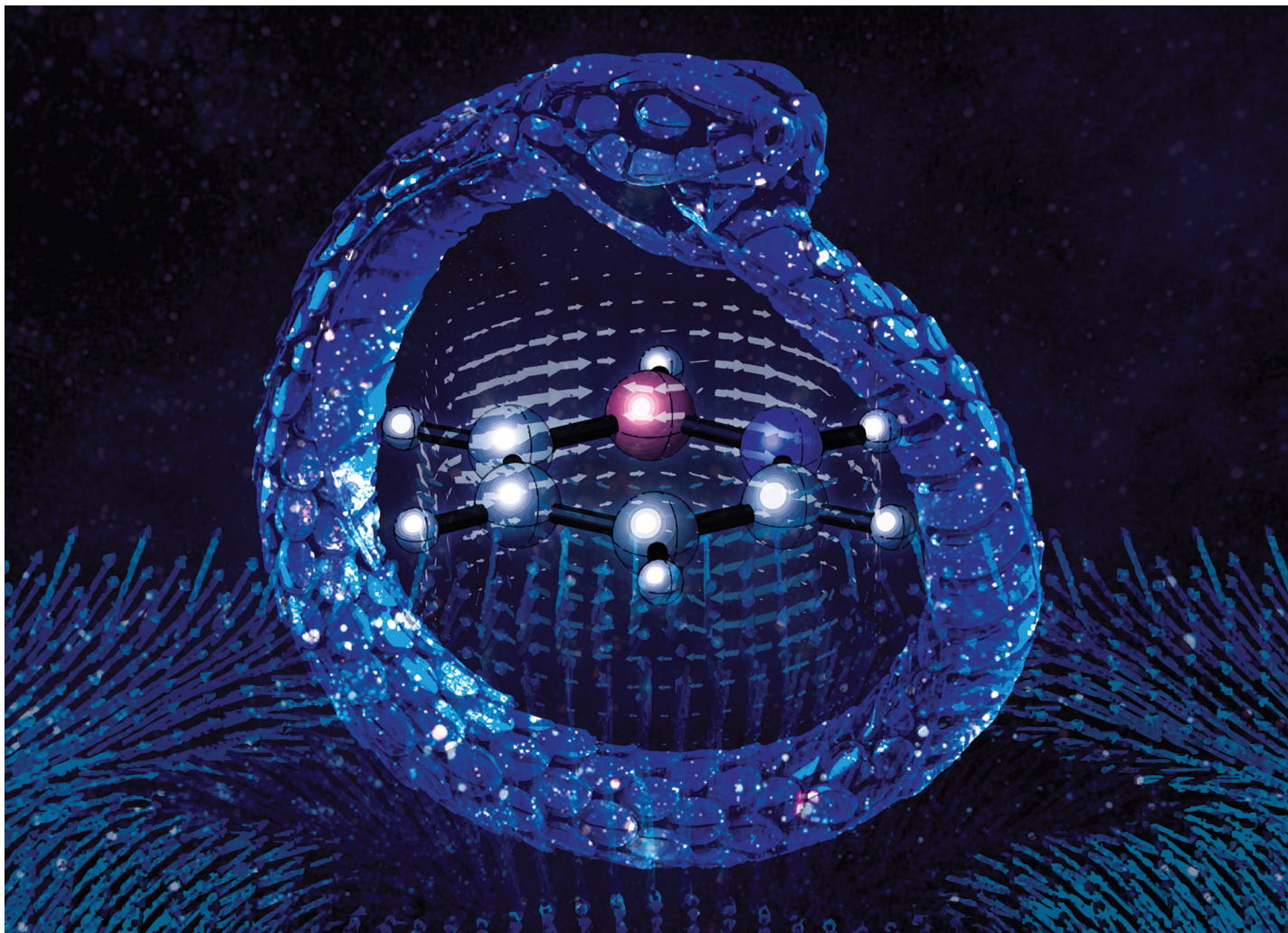
Follow this and additional works at: <https://scholarship.richmond.edu/chemistry-faculty-publications>

 Part of the [Chemistry Commons](#), and the [Physics Commons](#)

### Recommended Citation

Baez-Grez, Rodrigo, Diego Inostroza, Victor Garcia, Alejandro Vasquez-Espinal, Kelling J. Donald, and William Tiznado. "Aromatic Ouroboroi: Heterocycles Involving a Sigma-Donor-Acceptor Bond and  $4n+2$  Pi-Electrons." *Physical Chemistry Chemical Physics* 22, no. 4 (January 28, 2020): 1826–32. <https://doi.org/10.1039/c9cp05071j>.

This Article is brought to you for free and open access by the Chemistry at UR Scholarship Repository. It has been accepted for inclusion in Chemistry Faculty Publications by an authorized administrator of UR Scholarship Repository. For more information, please contact [scholarshiprepository@richmond.edu](mailto:scholarshiprepository@richmond.edu).



Showcasing research from the Groups of Prof. Kelling Donald at the University of Richmond, United States and Prof. William Tiznado at Universidad Andres Bello, Chile.

Aromatic ouroboroi: heterocycles involving a  $\sigma$ -donor-acceptor bond and  $4n + 2 \pi$ -electrons

A set of neutral heterocyclic systems were designed to have, potentially, six  $\pi$ -electrons. In allusion to Kekulé's dream, we refer to them as "ouroboroi", since the rings can be formed in principle by the coordination of a lone pair on an N, O, or F (electron donor) at one end of a simple chain (snake's tail) to a hypovalent B, Be or Mg site at the other end of that chain (snake's mouth).

As featured in:



See Kelling J. Donald, William Tiznado *et al.*, *Phys. Chem. Chem. Phys.*, 2020, 22, 1826.



Cite this: *Phys. Chem. Chem. Phys.*,  
2020, **22**, 1826

Received 13th September 2019,  
Accepted 1st December 2019

DOI: 10.1039/c9cp05071j

rsc.li/pccp

# Aromatic ouroboroi: heterocycles involving a $\sigma$ -donor–acceptor bond and $4n + 2$ $\pi$ -electrons†

Rodrigo Báez-Grez,<sup>a</sup> Diego Inostroza,<sup>a</sup> Víctor García,<sup>ab</sup>  
Alejandro Vásquez-Espinal,<sup>a</sup> Kelling J. Donald<sup>b,\*c</sup> and William Tiznado<sup>a</sup>

The aromaticity and dynamics of a set of recently proposed neutral 5- and 6-membered heterocycles that are closed by dative (donor–acceptor) or multi-center  $\sigma$  bonds, and have resonance forms with a Hückel number of  $\pi$ -electrons, are examined. The donors and acceptors in the rings include N, O, and F, and B, Be, and Mg, respectively. The planar geometry of the rings, coupled with evidence from different measures of aromaticity, namely the NICS<sub>zz</sub> and NICS<sub>zzz</sub> components of the conventional nucleus independent chemical shifts (NICS), and ring current strengths (RCS), indicate non-trivial degrees of aromaticity in certain cases, including the cyclic C<sub>3</sub>B<sub>2</sub>OH<sub>6</sub> and C<sub>3</sub>BOH<sub>5</sub> isomers, both with three bonds to the O site in the ring. The former is lower in energy by at least 17.6 kcal mol<sup>-1</sup> relative to linear alternatives obtained from molecular dynamics simulations in this work. Some of the other systems examined are best described as non-aromatic. Ring opening, closing, and isomerization are observed in molecular dynamics simulations for some of the systems studied. In a few cases, the ring indeed persists.

## Introduction

Since its introduction by August Kekulé in 1865,<sup>1–4</sup> the aromaticity concept has been used extensively for rationalizing chemical bonding, structure, stability, and molecular properties of chemical species in both organic and inorganic chemistry.<sup>5–10</sup> When Kekulé referred to the genesis of his theory, he stated that he came upon the ring shape of the benzene molecule after having a dream of a snake biting its own tail (imagery akin to the ancient *ouroboros*). Recently, one of us and collaborators<sup>11</sup> proposed a number of systems that – aligning more closely perhaps with the ouroboros metaphor – have unsaturated chains with valid Lewis structures that can cyclize *via* a  $\sigma$  dative (donor–acceptor, D  $\rightarrow$  A) bond coupled with  $\pi$ -delocalization. In such systems – consider, for example, F–CH=CH–CH=B–H – a lone pair on an N, O, or F (electron donor) at one end of the chain is donated into an empty orbital on B, Be or Mg (electron acceptor) at the other end to form a ring. The systems were designed to have, potentially, six  $\pi$ -electrons, in order to confer a degree of aromaticity on the ring in line with Hückel's  $4n + 2$  electron counting rule.<sup>12–14</sup>

Those types of ring systems are referred to in this work as “ouroboroi”.

Nucleus independent chemical shifts (NICS),<sup>15</sup> especially NICS<sub>zz</sub> rather than the isotropic NICS,<sup>16,17</sup> have been used to confirm the aromatic character of proposed species by comparison with the benzene molecule. Yet despite its popularity, many papers have identified inherent limitations of NICS as a measure of aromaticity.<sup>18–23</sup> There is no rigorous way, for example, (beyond a qualitative comparison with benzene) to use NICS to label borderline cases definitively as weakly aromatic *vs.* non-aromatic, or non-aromatic *vs.* slightly antiaromatic, and so on. Since the previous analysis of aromaticity in the systems was based only on NICS, we have performed herein a detailed analysis of the magnetically induced current density<sup>24–27</sup> in order to have an enhanced assessment of aromaticity according to magnetic criteria.

The strength of the magnetically induced current flows was compared with NICS values obtained under different approximations. Such analysis shows that both the out of plane component and the dissected  $\pi$  contributions of NICS correlate better with the information obtained from the current density analysis. This is consistent with the fact that the induced magnetic field ( $B^{\text{ind}}$ ), generated by a magnetic field applied perpendicular to the molecular plane, is more closely related to these properties. In turn,  $B^{\text{ind}}$  is connected to the induced current density through the Biot–Savart Law.<sup>28</sup>

Along with our assessment of the aromatic character of certain putative ouroboros-type ring systems, we evaluated the dynamic behavior of some of these species (to gain insights into their kinetic and thermodynamic stability), by means of

<sup>a</sup> Computational and Theoretical Chemistry Group, Departamento de Ciencias Químicas, Facultad de Ciencias Exactas, Universidad Andrés Bello, República 498, Santiago, Chile. E-mail: wtiznado@unab.cl

<sup>b</sup> Departamento Académico de Físicoquímica, Facultad de Química e Ingeniería Química, Universidad Nacional Mayor de San Marcos, Lima, Peru

<sup>c</sup> Department of Chemistry, Gottwald Center for the Sciences, University of Richmond, 28 Westhampton Way, Richmond, VA, 23173, USA. E-mail: kdonald@richmond.edu

† Electronic supplementary information (ESI) available. See DOI: 10.1039/c9cp05071j

Born–Oppenheimer molecular dynamic (BOMD) simulations.<sup>29</sup> This study elucidates the (non)aromatic character of the proposed systems and may serve as a guide towards designing new candidate ouroborei. The most aromatic of the cyclic species examined in this work are shown to persist in their cyclic rather than linear forms over the time window considered in the dynamics.

## Computational details

Geometry optimizations and vibrational frequency calculations were carried out at the B3LYP/cc-pVTZ<sup>30</sup> level using the Gaussian 16 computational package.<sup>31</sup>

NICS values were computed using the gauge-including atomic orbital (GIAO)<sup>32</sup> method and were dissected into their core,  $\sigma$  and  $\pi$  contributions using the natural chemical shielding (NCS)<sup>33</sup> analysis as implemented in the NBO 6.0 program,<sup>34</sup> at the B3LYP/cc-pVTZ level. To obtain NICS plots, the center of each molecule was placed on the origin of the Cartesian axes, with the molecular plane parallel to the  $xy$  Cartesian plane. Calculations of through-space NICS were performed in three-dimensional grids of points within a volume of  $10 \times 10 \times 10 \text{ \AA}^3$  with a step-size of  $0.2 \text{ \AA}$ . This approach makes it easier to extract the  $z$ -component of both NICS and induced magnetic field,  $B_z^{\text{ind}}$ , which are equivalent, as well as the vectorial expression  $\mathbf{B}^{\text{ind}}$ .<sup>16,35–38</sup> When the external magnetic field  $\mathbf{B}^{\text{ext}}$  is applied perpendicular to the molecular plane (*i.e.* along the  $z$ -axis), the  $xz$ ,  $yz$ , and  $zz$  components of the chemical shielding tensor at a specific point represent the  $x$ ,  $y$ , and  $z$  components of  $\mathbf{B}^{\text{ind}}$ , respectively.

Dynamic behavior was simulated using BOMD<sup>29</sup> computations at the B3LYP/Def2-SVP<sup>39</sup> level for 20 picoseconds (ps) with a time step of 1 fs. To ensure that the temperature remained constant (at 1200 K), it was verified that the nuclear kinetic energy remained constant throughout the simulation; to accomplish this, all velocities were rescaled at each step. These calculations were performed, using the Gaussian16 program.<sup>31</sup> Since this program only includes the velocity rescaling type of thermostat in the ADMP (atom centered density matrix propagation)<sup>40</sup> dynamics, the ADMP dynamics was run with the FULLSCF option, which is equivalent to a BOMD.

Current densities were computed with the GIMIC program<sup>25,41</sup> using the gauge including atomic orbitals (GIAO)<sup>32</sup> method. In the calculations, the magnetic field is directed along the  $z$ -axis, *i.e.* perpendicularly to the molecular plane. The unit for the current susceptibility is  $\text{nA T}^{-1}$  and the results are thus independent of the magnetic field magnitude. For a qualitative analysis, vector plots of the current density in a plane placed  $0.0$  and  $0.5 \text{ \AA}$  above the molecular plane were generated. Diatropic (aromatic) and paratropic (antiaromatic) currents are assumed to circle clockwise and counterclockwise, respectively. Current pathways are visualized using Paraview.<sup>42,43</sup> Explicit values for ring-current strengths (RCS) are obtained by numerical integration of the current density passing through cut planes perpendicular to selected bonds of the molecular system (see Fig. S1, ESI<sup>†</sup>). In these systems, the integration planes extend about  $3.8 \text{ \AA}$  horizontally along the plane of the ring, with  $2.6 \text{ \AA}$  above and  $2.6 \text{ \AA}$  below the ring. The two-dimensional

Gauss–Lobatto algorithm<sup>41,44</sup> was used to integrate the current that passes through an integration plane. Diatropic and paratropic contributions were considered to compute net RCSs. The sign and magnitude of RCS indicate whether molecular rings are aromatic, antiaromatic, or nonaromatic, thus having diatropic (positive), paratropic (negative), or vanishing (close to zero) net ring currents, respectively.<sup>24</sup>

## Results and discussion

The systems studied are depicted in Fig. 1 (for the coordinates of the optimized systems see Table S1, ESI<sup>†</sup>). All of them have at least one resonance form that would fulfill the  $4n + 2 \pi$ -electron rule, and have been labelled with numbers and arranged in subgroups according to size and the nature of the acceptor/donor atoms used to close the rings. Systems 1 and 2 (not shown) are benzene ( $\text{C}_6\text{H}_6$ ) and the cyclopentadienyl anion ( $\text{C}_5\text{H}_5^-$ ), respectively, which are used as references in assessing the aromaticity of the cyclic systems. We will begin by comparing ring current strengths (RCSs) with the out-of-plane component of the NICS tensor (commonly represented as  $\text{NICS}_{zz}$ ), suggested by Fowler and Steiner in 2000 as an improved aromaticity index.<sup>45,46</sup> The isotropic NICS were not considered in this study since it is well documented that it does not (conceptually) represent Pople's ring currents.<sup>47,48</sup> Additionally,  $\text{NICS}_{zz}$  values are particularly sensitive to cyclic  $\pi$ -electron delocalization, so,  $\text{NICS}_{zz}$  are expected to provide the best correlation with  $\pi$ -current densities associated with the aromaticity phenomenon in these species.

The  $\text{NICS}_{zz}$  and  $\text{NICS}_{\pi zz}$  ( $\pi$  contribution to  $\text{NICS}_{zz}$ ) computations were performed at the center ( $0.0 \text{ \AA}$ ) and at different distances ( $1.0 \text{ \AA}$ ,  $1.4 \text{ \AA}$  and  $2.0 \text{ \AA}$ ) above the molecular rings. The values obtained are reported in Table 1 ( $\text{NICS}_{zz}$ ) and Table 2 ( $\text{NICS}_{\pi zz}$ ). In both tables the RCS values are also reported for comparison. Table S2 (ESI<sup>†</sup>) shows RCSs for all systems as an average of computed net RCSs for each bond of the ring. At this point, it is important to mention that for these two properties opposite signs are assigned to aromatic or antiaromatic molecules. A negative sign (diatropic) and a positive sign (paratropic) for NICS correspond to aromatic and antiaromatic profiles, respectively, for molecules,

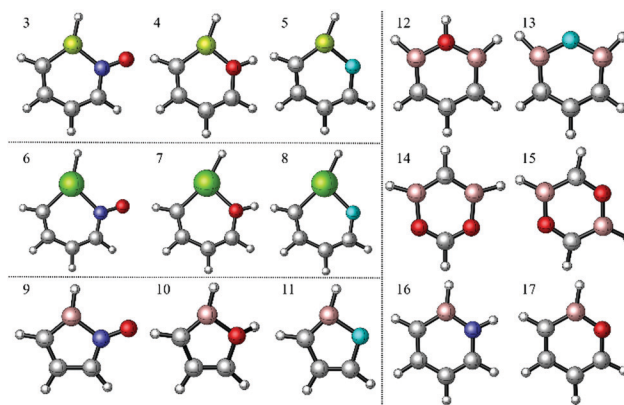


Fig. 1 Molecules analyzed. Atom colors: yellow green Be, blue N, red O, light blue F, green Mg, pink B, gray C and white H.

**Table 1** Comparison of RCS with different NICS<sub>zz</sub> computations, for the molecules studied. \* Cases where the two approaches differ on the aromatic character of species are indicated by an asterisk

System	RCS [nA T <sup>-1</sup> ]	NICS <sub>zz</sub> [ppm]			
		0.0 Å	1.0 Å	1.4 Å	2.0 Å
1 C <sub>6</sub> H <sub>6</sub>	12.2	-16.0	-29.8	-26.3	-17.5
2 C <sub>5</sub> H <sub>5</sub> <sup>-</sup>	12.9	-18.2	-34.2	-28.5	-17.8
3 C <sub>4</sub> BeH <sub>5</sub> NO	-1.9	24.1	8.7	2.5	-1.4
4 C <sub>4</sub> BeOH <sub>6</sub>	2.2	12.4*	-3.1	-6.2	-6.1
5 C <sub>4</sub> BeFH <sub>5</sub>	1.1	15.3*	-0.2	-3.9	-4.7
6 C <sub>4</sub> MgH <sub>5</sub> NO	-0.8	15.8	4.7	0.8	-1.7*
7 C <sub>4</sub> MgOH <sub>6</sub>	0.9	14.2*	1.3*	-2.4	-3.9
8 C <sub>4</sub> MgFH <sub>5</sub>	0.5	15.3*	2.2*	-1.6	-3.3
9 C <sub>3</sub> BH <sub>4</sub> NO	-9.8	39.8	23.3	11.5	3.0
10 C <sub>3</sub> BOH <sub>5</sub>	6.7	0.7*	-15.9	-14.8	-10.2
11 C <sub>3</sub> BFH <sub>4</sub>	4.9	3.5*	-11.2	-11.1	-8.0
12 C <sub>3</sub> B <sub>2</sub> OH <sub>6</sub>	5.0	3.7*	-10.6	-11.7	-9.3
13 C <sub>3</sub> B <sub>2</sub> FH <sub>5</sub>	3.1	9.3*	-5.3	-7.7	-6.9
14 (i) C <sub>2</sub> B <sub>2</sub> O <sub>2</sub> H <sub>4</sub>	5.0	5.0*	-11.5	-12.2	-9.2
15 (ii) C <sub>2</sub> B <sub>2</sub> O <sub>2</sub> H <sub>4</sub>	7.8	-5.9	-19.8	-17.9	-12.0
16 C <sub>4</sub> BNH <sub>6</sub>	8.9	-6.2	-20.9	-19.7	-13.8
17 C <sub>4</sub> BOH <sub>5</sub>	7.1	-1.3	-16.8	-16.4	-11.8

**Table 2** Comparison of RCS with different NICS<sub>πzz</sub> computations, for the molecules studied

System	RCS [nA T <sup>-1</sup> ]	NICS <sub>πzz</sub> [ppm]			
		0.0 Å	1.0 Å	1.4 Å	2.0 Å
1 C <sub>6</sub> H <sub>6</sub>	12.2	-36.8	-29.8	-22.4	-13.1
2 C <sub>5</sub> H <sub>5</sub> <sup>-</sup>	12.9	-35.9	-29.3	-21.4	-12
3 C <sub>4</sub> BeH <sub>5</sub> NO	-1.9	7.9	7.7	4.7	1.6
4 C <sub>4</sub> BeOH <sub>6</sub>	2.2	-5.8	-4.3	-4.0	-3.0
5 C <sub>4</sub> BeFH <sub>5</sub>	1.1	-2.3	-1.3	-1.7	-1.8
6 C <sub>4</sub> MgH <sub>5</sub> NO	-0.8	3.5	3.4	2.0	0.6
7 C <sub>4</sub> MgOH <sub>6</sub>	0.9	-1.4	-1.3	-1.5	-1.5
8 C <sub>4</sub> MgFH <sub>5</sub>	0.5	-0.1	0.0	-0.5	-0.9
9 C <sub>3</sub> BH <sub>4</sub> NO	-9.8	32.9	27.4	16.4	7.1
10 C <sub>3</sub> BOH <sub>5</sub>	6.7	-12.5	-9.9	-7.5	-4.6
11 C <sub>3</sub> BFH <sub>4</sub>	4.9	-8.9	-5.9	-4.9	-3.3
12 C <sub>3</sub> B <sub>2</sub> OH <sub>6</sub>	5.0	-15.0	-11.5	-9.07	-5.9
13 C <sub>3</sub> B <sub>2</sub> FH <sub>5</sub>	3.1	-8.8	-5.9	-5.01	-3.6
14 (i) C <sub>2</sub> B <sub>2</sub> O <sub>2</sub> H <sub>4</sub>	5.0	-14.9	-11.3	-8.9	-5.6
15 (ii) C <sub>2</sub> B <sub>2</sub> O <sub>2</sub> H <sub>4</sub>	7.8	-25.3	-19.8	-14.7	-8.6
16 C <sub>4</sub> BNH <sub>6</sub>	8.9	-26.4	-21.3	-16.3	-9.8
17 C <sub>4</sub> BOH <sub>5</sub>	7.1	-21.5	-16.9	-12.9	-7.9

whereas positive (diatropic) and negative (paratropic) RCSs correspond to aromatic and antiaromatic molecules, respectively. For both NICS and RCS, however, values close to zero suggest marginal or nonaromatic behavior.

A first analysis involved identifying the cases where NICS and RCS disagree with the (anti)aromatic classification for certain molecules, such as cases where NICS predicts an aromatic character and RCS predicts the contrary. In this work, that only happens when the global NICS<sub>zz</sub> values are considered, the specific cases have been noted by an asterisk in Table 1. Disagreement occurs in nine cases for NICS<sub>zz</sub>(0.0), two cases for NICS<sub>zz</sub>(1.0) and one case for NICS<sub>zz</sub>(2.0). The increasing disagreement between NICS<sub>zz</sub> and RCS values, as NICS<sub>zz</sub> is computed closer to the plane evidences the influence of local contributions to NICS<sub>zz</sub>, which are expected to be more pronounced at the molecular center. The discrepancies between RCSs and NICS disappear, however,

when the dissected NICS<sub>πzz</sub> are analyzed (see Table 2). The borderline cases, very marginal (anti)aromatic or non-aromatic, are considered in the same category (non-aromatic) to simplify this analysis.

The relationship between RCS and NICS, for the systems that we have analyzed, is represented in the scatter plots displayed in Fig. 2. In this figure, the NICS values have been multiplied by -1 and, like RCS, they have been normalized by dividing them by the value obtained for the most aromatic species. The NICS<sub>zz</sub>(0.0) values (see Fig. S2, ESI<sup>†</sup>) correlate very well with RCSs ( $R^2 = 0.99$ ), but we do not include that line in Fig. 2a since that line is noticeably steeper compared to the other NICS<sub>zz</sub> lines. However, it is clear from the graphs (Fig. S2, ESI<sup>†</sup>) that despite the high correlation, the NICS<sub>zz</sub>(0.0) line falls far from the  $y = x$  line (in black). This is because while systems 6, 7 and 8, are classified by NICS<sub>zz</sub>(0.0), for instance, as antiaromatic with high paratropic values (~15 ppm) they are classified as nonaromatic by RCS. The other lines cluster around the  $y = x$  reference, however, affirming a more reliable correspondence between NICS<sub>zz</sub> and RCS in those cases. The best correlations between NICS and RCSs in Fig. 2 are found for NICS<sub>zz</sub>(1.0), NICS<sub>πzz</sub>(0.0), and NICS<sub>πzz</sub>(1.0), with  $R^2 = 0.98$ , but the correspondence is still high for the other cases in Fig. 2 as well, with  $R^2 \geq 0.95$ .

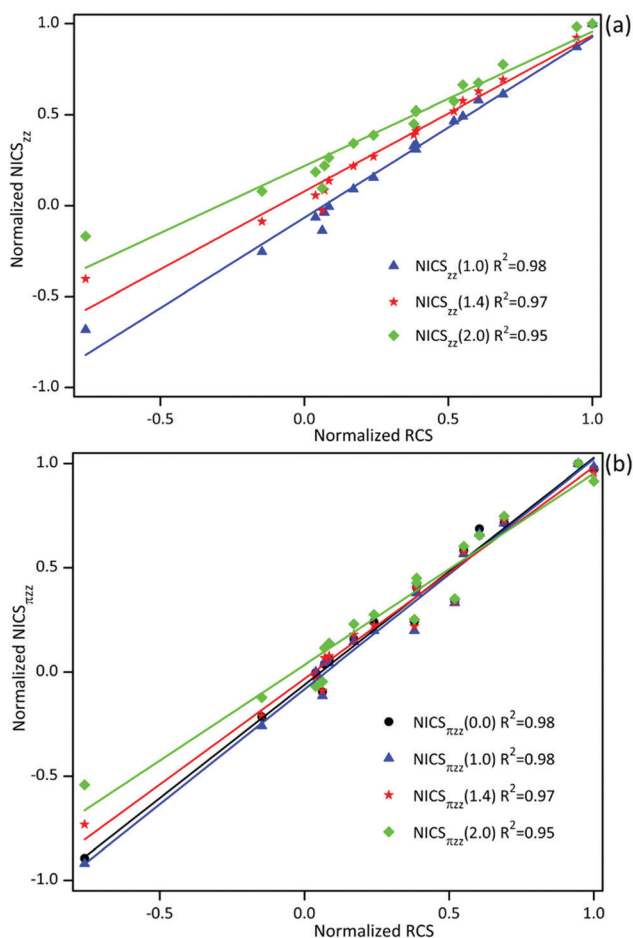


**Fig. 2** Plots of (a) normalized NICS<sub>zz</sub> vs. normalized RCS values and, (b) normalized NICS<sub>πzz</sub> vs. normalized RCS values.

Given the demonstrated agreement between the two methods for assessing aromaticity, what, one might ask, is the value to using both in our analysis? One reason is to demonstrate the usefulness of the RCS, which is underutilized compared to NICS as a measure of aromaticity, and to use this opportunity as well to highlight strengths of both approaches.

Note that RCSs were obtained as an average, considering different integration planes (see Fig. S1, ESI<sup>†</sup>), aiming to estimate the net intensity of the ring current flow on the heterocyclic rings. In this context, it is important to mention that ring current analysis provides the possibility of scrutinizing those cases that are suspected as problematic, *e.g.* by inspection of the ring current maps and (or) using critical points of the current density module as a reference to place the integration planes. On the other hand, a 2D or 3D analysis of NICS also provides additional information to analyze aromaticity of difficult systems such as those analyzed here. To illustrate the strategy, we will focus on systems **10** ( $C_3BOH_5$ ) and **11** ( $C_3BFH_4$ ). These systems have been selected for further analysis as they have characteristics that could lead to gross errors with NICS predictions about their aromaticity. Both are 5-membered rings (analogous to the cyclopentadienyl anion); hence, they are smaller and more constrained than the 6-member rings. Additionally, they feature highly polar B–O and B–F bonds and, unlike  $C_4BNH_6$ , do not have simple Lewis structures to account for  $\sigma$  bonding. Fig. 3 shows vector plots of the induced current density (both in the molecular plane and in a plane 0.5 Å above and parallel to it) and a picture of a 3D map of the induced magnetic field vectors,  $B^{ind}$ . Ring currents and  $B^{ind}$  are induced by an external

magnetic field applied in a direction perpendicular to the molecular ring (from bottom to top for the  $B^{ind}$  showed in Fig. 3b).

As can be seen in Fig. 3, the diatropic induced ring current in Fig. 3a (clockwise arrows) produce the anisotropic effects of the induced magnetic field that are characteristic for aromatic compounds: an inverted diatropic cone shape towards the center of the molecule, where  $B^{ind}$  is opposed to the applied field (shielding zone in blue) and, a paratropic region, where  $B^{ind}$  is parallel to the applied field, outside of the molecular ring (deshielding zone in red). Vector plots of the current density for all systems studied are depicted in Fig. S3, ESI<sup>†</sup>. These results are in complete agreement with the quantitative correlation between  $NICS_{zz}$  and RCS (Fig. 2).

We should mention here that system **10** is not completely flat. The O–H bond is out of the plane of the ring with a dihedral angle between the HBO and BOH planes of about  $38^\circ$ . Consequently, a p-orbital on O that is normally involved fully in the  $\pi$ -system – see HOMO–1 at the top in Fig. 4 – is somewhat twisted, such that it is partially  $\sigma$  and partially  $\pi$  relative to the rest of MO. For both systems **10** and **11**, three occupied frontier  $\pi$ -MOs are shown in Fig. 4. The distortion in **10** is evidently an outcome of the electron density polarization at the O atom due to the relative electronegativity and an effort toward optimal overlap of the O and B atoms in the molecule. As a consequence of those influences, and consistent with previous studies,<sup>16,38</sup> RCSs is considered the best quantitative assessment of the aromatic character of the species that we consider in this work.

Systems with RCS values greater than  $1.0 \text{ nA T}^{-1}$  have been selected to evaluate their dynamic behaviour through

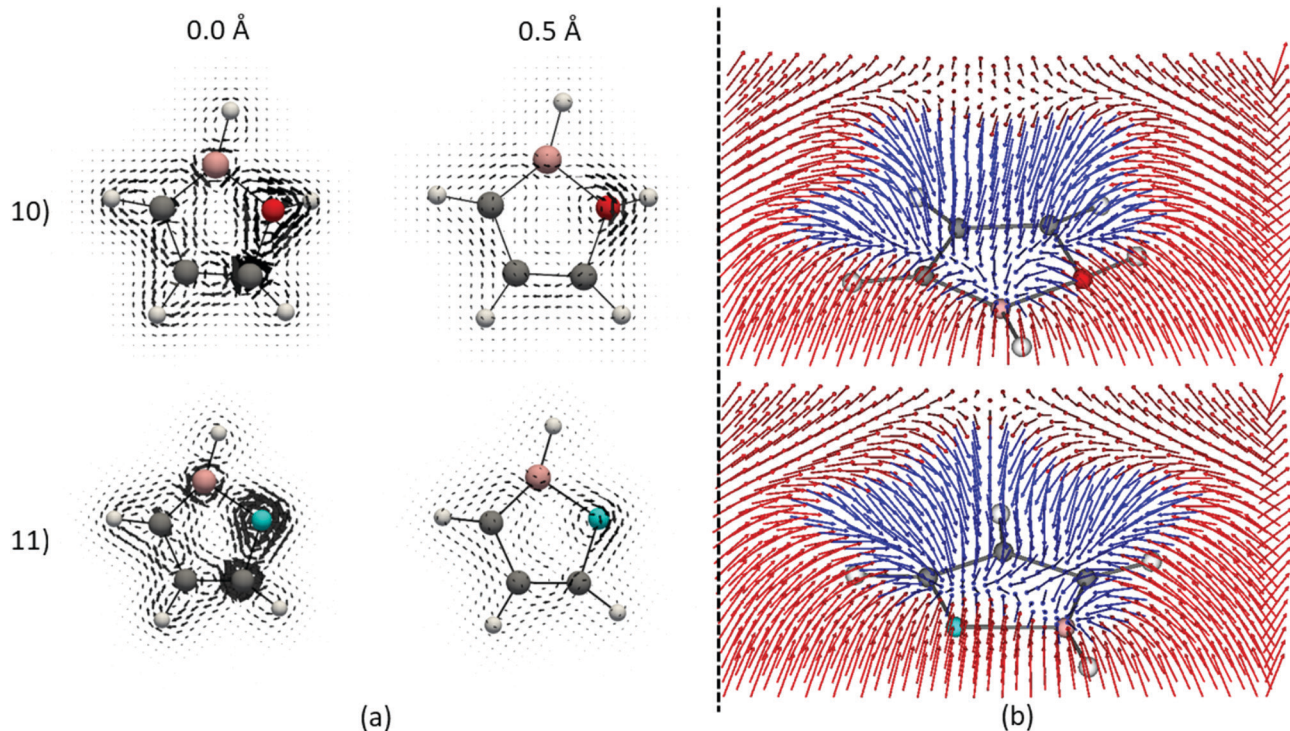


Fig. 3 Vector plot visualization of the current density (a) and the induced magnetic field (b) of systems **10** and **11**. The current density is plotted in a plane at 0.0 Å and in a plane at 0.5 Å above the molecular plane. the colour of the atoms is the same as used in Fig. 1.

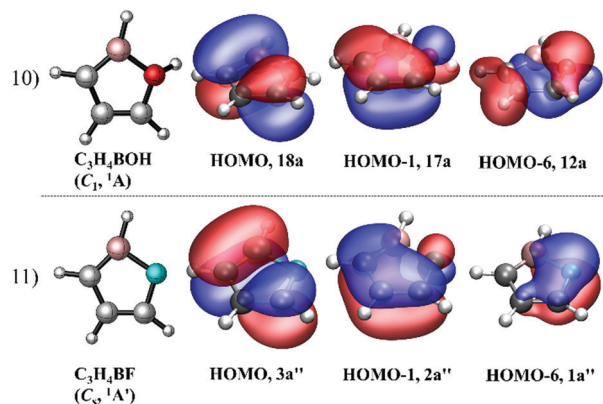


Fig. 4 Valence  $\pi$  molecular orbitals of systems **10** and **11**.

BOMD simulations.<sup>29</sup> The corresponding movies are available in the ESI.† We find that if we start from their ring structures, the cyclic arrangement persists over the period of time considered for the dynamics (20 ps) for the **12**, **14**, **15**, **16** and **17** systems. Interestingly, these systems are the most aromatic (the corresponding RCS values are equal to or greater than 41% of that of benzene) among all those studied. In the case of system **10**, the RCS reaches 55% of that of benzene, but its ring opens simultaneously with the transfer of an H from a neighbouring C to B (within 4 ps), and that open chain structure persists throughout the period considered for the dynamics (20 ps).

According to the RCSs data, the most aromatic of molecules 3–17 are **10**, **15**, **16** and **17**, whose RCS values (Table 2) reach 55%, 64%, 73% and 58% of the benzene RCS, respectively.

To complement the above results, we performed new dynamic simulations for systems **12**, **14**, **15**, **16** and **17**, starting in this second case from their linear forms instead. In those simulations, system **16** ( $C_4BNH_6$ ) quickly adopted the ring shape (within approximately 5 ps) and maintained its cyclic form through to the end of the dynamic simulation (see Fig. 5a and b). We found that species **16** adopted two annular forms during the dynamics study before arriving at the six-membered ring form: it forms first a four-membered ( $\overrightarrow{C-C-C-B}$ ) ring, which is followed by a bicyclic structure with an N–B bond, which transforms readily into the single six-membered ring that persists until the end of the simulation. This result provides support for the kinetic and thermodynamic stability of **16**.

Other interesting results have been obtained from the dynamics studies on systems **12**, **14**, **15** and **17**. System **12** forms first a three-membered ( $\overrightarrow{C-C-B}$ ) ring with the migration of an H from C to B, this ring opens, and the open chain shape persists until the end of the dynamics. For system **14**, a H atom is transferred from a neighbouring C to the B (at the beginning of the dynamics), but within 15 ps a cyclic structure is formed which opens immediately to the starting linear structure. System **15** evolves from the linear to a branched structure (more stable than the ring-shaped isomer) with a central carbon atom bonded to four different groups ( $-H$ ,  $-B=O$ ,  $-CH=O$  and  $-BH_2$ ), as depicted in Fig. S4 and Table S3 in the ESI.† System **17**, adopts two annular

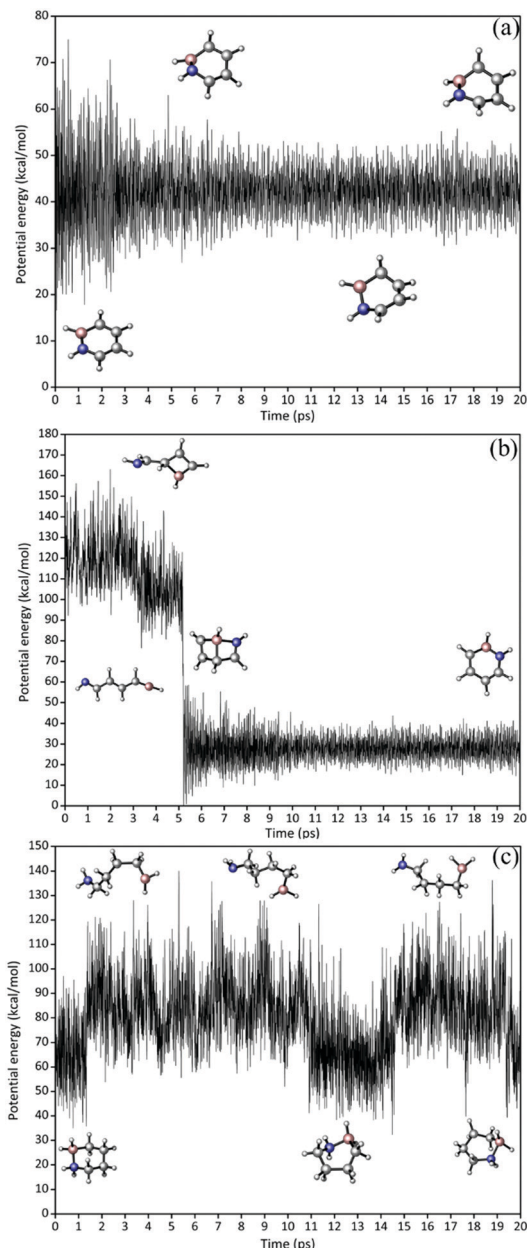


Fig. 5 Potential energy profiles showing molecular structural changes along the BOMD simulation for (a) an unsaturated (system **16**), (b) linear, and (c) a saturated case.

forms during the dynamics study, the first is a four-membered ring ( $\overrightarrow{C-C-C-B}$ ), which opens and forms a five-membered ring ( $\overrightarrow{O-C-C-C-C}$ ) that persists until the end of the simulation (see Fig. S4, ESI†).

What about saturated ourboroi? We have focused in this work on the unsaturated species for reasons outlined above, but we evaluated the hydrogenated analogue of system **16** as well, and the corresponding energetic profile of the BOMD is shown in Fig. 5c. Both the cyclic and open chain forms appear along the dynamics simulation, with a preference for the ring form over the chain, which is in line with the observation in

ref. 11 where  $\Delta G$  for cyclization was computationally found to be  $-28.80 \text{ kcal mol}^{-1}$ .

## Conclusions

The aromaticity of a series of 5- and 6-membered heterocycles that can be generated from chain forms by donor–acceptor bonding – without  $\sigma$ -bond breaking – to give potentially aromatic rings was evaluated. For these systems, both the chain and the ring forms have formally valid Lewis structures, but cyclization is driven by dative bond formation between acceptor (A = B, Be, and Mg) and donor (D = N, O, and F) atoms at the ends of the chains – a mode of ring closure (D  $\rightarrow$  A) analogous to the ancient ouroboros. In addition to  $\sigma$  donor–acceptor bond formation and subsequent electron redistribution in the  $\sigma$ -skeleton of the ring, the stability and planarity of the ring is favored by  $\pi$ -delocalization in a number of cases. We assessed in detail the extent of the aromaticity in the full slate of molecules using, as our criteria, relevant components of the conventional nucleus independent chemical shift (NICS), and the related ring current strengths (RCS).

Our analyses confirm that (like the better-known case – 1,2-dihydro-1,2-azaborine) some of the novel cases – including the  $\text{C}_3\text{BOH}_5$  and  $\text{C}_3\text{BO}_2\text{H}_6$  rings, both with three  $\sigma$  bonds to the O site – exhibit non-trivial degrees of aromaticity. The dynamics of the molecules with noticeable aromatic character were assessed. In some cases, the cyclization is rather easily reversed (especially when D = F) even if the ring is more stable thermodynamically than chain forms. In a few cases, however, the ring form persists for the full duration of the dynamics. Strategies for enhancing the aromaticity of self-cyclizing or ouroboros-type rings have not been sought in this investigation. We demonstrate a close correspondence between RCS with both (i)  $\text{NICS}_{zz}$  beyond (but not at) ring center and (ii)  $\text{NICS}_{\pi zz}$  as measures of aromaticity, especially when they are all normalized with respect to a common reference (benzene in this case). Both approaches confirm a role for aromaticity in stabilizing a diverse subset of unusual heterocycles.

## Conflicts of interest

There are no conflicts to declare.

## Acknowledgements

The authors are grateful for the financial support of the Fondcyt Grant No. 1181165. K. J. D. acknowledges the support of the University of Richmond and the Henry Dreyfus Teacher-Scholar Awards Program.

## References

- 1 A. Kekulé, *Bull. Mens. la Société Chim. Paris*, 1865, **3**, 98–110.
- 2 A. Kekulé, *Bull. Acad. R. Med. Belg.*, 1865, **19**, 551–563.
- 3 A. Kekulé, *Annal. der Chem. und Pharm.*, 1866, **137**, 129–196. (currently available at: *Eur. J. Org. Chem.*, 1866, **137**, 129–196.).
- 4 A. Kekulé, *Annal. der Chem. und Pharm.*, 1872, **162**, 77–124. (currently available at: *Eur. J. Org. Chem.*, 1872, **162**, 77–124.).
- 5 P. von R. Schleyer, *Chem. Rev.*, 2001, **101**, 1115–1118.
- 6 J. Gomes and R. B. Mallion, *Chem. Rev.*, 2001, **101**, 1349–1384.
- 7 M. Randić, *Chem. Rev.*, 2003, **103**, 3449–3606.
- 8 A. P. Sergeeva, B. B. Averkiev and A. I. Boldyrev, *Metal-Metal Bonding*, Springer, 2010, pp. 275–305.
- 9 T. M. Krygowski and M. K. Cyrański, *Chem. Rev.*, 2001, **101**, 1385–1420.
- 10 P. K. Chattaraj, *Aromaticity and Metal clusters*, CRC Press, 2010.
- 11 K. J. Donald, S. Gillespie and Z. Shafi, *Tetrahedron*, 2019, **75**, 335–345.
- 12 E. Hückel, *Z. Phys.*, 1930, **60**, 423–456.
- 13 E. Hückel, *Z. Phys.*, 1931, **70**, 204–286.
- 14 E. Hückel, *Z. Phys.*, 1931, **72**, 310–337.
- 15 P. von, R. Schleyer, C. Maerker, A. Dransfeld, H. Jiao and N. J. R. van E. Hommes, *J. Am. Chem. Soc.*, 1996, **118**, 6317–6318.
- 16 R. Báez-Grez, L. Ruiz, R. Pino-Rios and W. Tiznado, *RSC Adv.*, 2018, **8**, 13446–13453.
- 17 C. Corminboeuf, T. Heine, G. Seifert, P. von Ragué Schleyer and J. Weber, *Phys. Chem. Chem. Phys.*, 2004, **6**, 273–276.
- 18 C. Foroutan-Nejad, *Theor. Chem. Acc.*, 2015, **134**, 1–9.
- 19 S. Pelloni, G. Monaco, P. Lazzeretti and R. Zanasi, *Phys. Chem. Chem. Phys.*, 2011, **13**, 20666–20672.
- 20 R. Islas, G. Martínez-Guajardo, J. O. C. Jiménez-Halla, M. Solà and G. Merino, *J. Chem. Theory Comput.*, 2010, **6**, 1131–1135.
- 21 J. Poater, M. Solà, R. G. Viglione and R. Zanasi, *J. Org. Chem.*, 2004, **69**, 7537–7542.
- 22 J. J. Torres, R. Islas, E. Osorio, J. G. Harrison, W. Tiznado and G. Merino, *J. Phys. Chem. A*, 2013, **117**, 5529–5533.
- 23 M. Solà, F. Feixas, J. O. C. Jiménez-Halla, E. Matito and J. Poater, *Symmetry*, 2010, **2**, 1156–1179.
- 24 D. Sundholm, H. Fliegl and R. J. F. Berger, *Wiley Interdiscip. Rev.: Comput. Mol. Sci.*, 2016, **6**, 639–678.
- 25 H. Fliegl, S. Taubert, O. Lehtonen and D. Sundholm, *Phys. Chem. Chem. Phys.*, 2011, **13**, 20500–20518.
- 26 P. Lazzeretti, *Prog. Nucl. Magn. Reson. Spectrosc.*, 2000, **36**, 1–88.
- 27 P. Lazzeretti, *Phys. Chem. Chem. Phys.*, 2004, **6**, 217–223.
- 28 T. Heine, C. Corminboeuf and G. Seifert, *Chem. Rev.*, 2005, **105**, 3889–3910.
- 29 J. M. Millam, V. Bakken, W. Chen, W. L. Hase and H. B. Schlegel, *J. Chem. Phys.*, 1999, **111**, 3800–3805.
- 30 R. A. Kendall, T. H. Dunning Jr and R. J. Harrison, *J. Chem. Phys.*, 1992, **96**, 6796–6806.
- 31 M. J. Frisch, G. W. Trucks, H. B. Schlegel, G. E. Scuseria, M. A. Robb, J. R. Cheeseman, G. Scalmani, V. Barone, G. A. Petersson, H. Nakatsuji, X. Li, M. Caricato, A. V. Marenich, J. Bloino, B. G. Janesko, R. Gomperts, B. Mennucci, H. P. Hratchian, J. V. Ortiz, A. F. Izmaylov, J. L. Sonnenberg, D. Williams-Young, F. Ding, F. Lipparini, F. Egidi, J. Goings, B. Peng, A. Petrone, T. Henderson, D. Ranasinghe, V. G. Zakrzewski, J. Gao, N. Rega, G. Zheng, W. Liang, M. Hada, M. Ehara, K. Toyota, R. Fukuda, J. Hasegawa, M. Ishida, T. Nakajima, Y. Honda, O. Kitao, H. Nakai, T. Vreven,

- K. Throssell, J. A. Montgomery, Jr., J. E. Peralta, F. Ogliaro, M. J. Bearpark, J. J. Heyd, E. N. Brothers, K. N. Kudin, V. N. Staroverov, T. A. Keith, R. Kobayashi, J. Normand, K. Raghavachari, A. P. Rendell, J. C. Burant, S. S. Iyengar, J. Tomasi, M. Cossi, J. M. Millam, M. Klene, C. Adamo, R. Cammi, J. W. Ochterski, R. L. Martin, K. Morokuma, O. Farkas, J. B. Foresman and D. J. Fox, *Gaussian 16, Revision B.01*, Gaussian, Inc., Wallingford CT, 2016.
- 32 K. Wolinski, J. F. Hinton and P. Pulay, *J. Am. Chem. Soc.*, 1990, **112**, 8251–8260.
- 33 J. A. Bohmann, F. Weinhold and T. C. Farrar, *J. Chem. Phys.*, 1997, **107**, 1173–1184.
- 34 E. D. Glendening, J. K. Badenhoop, A. E. Reed, J. E. Carpenter, J. A. Bohmann, C. M. Morales, C. R. Landis and F. Weinhold, *NBO 6.0*, Theoretical Chemistry Institute, University of Wisconsin, Madison, 2013.
- 35 J. J. Torres-Vega, A. Vásquez-Espinal, J. Caballero, M. L. Valenzuela, L. Alvarez-Thon, E. Osorio and W. Tiznado, *Inorg. Chem.*, 2014, **53**, 3579–3585.
- 36 A. Vásquez-Espinal, R. Pino-Rios, L. Alvarez-Thon, W. A. Rabanal-León, J. J. Torres-Vega, R. Arratia-Perez and W. Tiznado, *J. Phys. Chem. Lett.*, 2015, **6**, 4326–4330.
- 37 R. Pino-Rios, G. Cárdenas-Jirón, L. Ruiz and W. Tiznado, *ChemistryOpen*, 2019, **8**, 321–326.
- 38 R. Báez-Grez, W. A. Rabanal-León, L. Alvarez-Thon, L. Ruiz, W. Tiznado and R. Pino-Rios, *J. Phys. Org. Chem.*, 2019, **32**, e3823.
- 39 F. Weigend and R. Ahlrichs, *Phys. Chem. Chem. Phys.*, 2005, **7**, 3297–3305.
- 40 H. B. Schlegel, J. M. Millam, S. S. Iyengar, G. A. Voth, A. D. Daniels, G. E. Scuseria and M. J. Frisch, *J. Chem. Phys.*, 2001, **114**, 9758–9763.
- 41 J. Jusélius, D. Sundholm and J. Gauss, *J. Chem. Phys.*, 2004, **121**, 3952–3963.
- 42 J. Ahrens, B. Geveci and C. Law, Paraview: An end-user tool for large data visualization, *The Visualization Handbook*, Elsevier, 2005, vol. 717.
- 43 U. Ayachit, *The ParaView Guide: A Parallel Visualization Application*, Kitware, Inc., USA, 2015.
- 44 M. Abramowitz, *Handbook of Mathematical Functions, With Formulas, Graphs, and Mathematical Tables*, Dover Publications, Inc., New York, NY, USA, 1974.
- 45 I. Cernusak, P. W. Fowler and E. Steiner, *Mol. Phys.*, 2000, **98**, 945–953.
- 46 E. Steiner, P. W. Fowler and L. W. Jenneskens, *Angew. Chem., Int. Ed.*, 2001, **40**, 362–366.
- 47 J. A. Pople, *Mol. Phys.*, 1958, **1**, 175–180.
- 48 H. Fallah-Bagher-Shaidaei, C. S. Wannere, C. Corminboeuf, R. Puchta and P. v. R. Schleyer, *Org. Lett.*, 2006, **8**, 863–866.